

# Emulator Design and Generation of Synthetic Dataset in Multi-Ion Sensing

Ivan Ny Hanitra<sup>\*†</sup>, Danilo Demarchi<sup>‡</sup>, Sandro Carrara<sup>†</sup> and Giovanni De Micheli<sup>†</sup>

<sup>\*</sup>Corresponding author: ivan.nyhanitra@epfl.ch

<sup>†</sup>Integrated Systems Laboratory, EPFL, Switzerland

<sup>‡</sup>Department of Electronics and Telecommunications, Politecnico di Torino, Italy

**Abstract**—Multi-ion potentiometric sensing becomes challenging for mixed-ion samples in which interfering electrolytes significantly alter the response of each single sensor. Therefore, an emulator based on the phase-boundary potential model is proposed to simulate multi-ion sensing in presence of interference. It serves as investigation tool for understanding the impact of sensor selectivity and interferent ions in the sensor response. Moreover, the emulator is used to design mixed-ion synthetic dataset, following a multi-factorial design of ion mixtures with orthogonal arrays. Such large dataset is suitable for data-intensive learning algorithms used in multivariate calibration of potentiometric sensor arrays.

**Index Terms**—Mixed-ion potentiometric sensing, Phase-boundary potential model, Calibration-curve emulator, Orthogonal design of experiments

## I. INTRODUCTION

Potentiometric ion sensors are ubiquitous in healthcare monitoring and wearable physiology, enabling the detection of a wide range of electrolytes [1]. This could be done in a non-invasive way, through biological fluids such as sweat [2]. The main minerals present in perspiration are sodium, chloride, potassium, and in weaker amount, calcium [3]. Following an intensive physical exercise, depletion of potassium and sodium could lead to dehydration, muscle cramps, or to more severe physiological dysfunctions such as hypokalemia and hyponatremia [4]. In addition, calcium levels indicate bone mineral loss [5], and other ions are monitored in order to control electrolyte balance. Moreover, human body excretes trace metals in sweat such as zinc, iron, or lead, whose concentration may change due to exposure to contaminated food, dust, or gasoline [6]. Other exogenous electrolytes could be present in sweat, as for example lithium, that is prescribed for people suffering from mental disorder [7].

All-solid-state sensing technology together with progress in microtechnology and electronics enable the integration of multi-ion sensors into wearable systems [1] [8]. One of the main challenge in multi-electrolyte monitoring comes from the impact of interferent ions in sensor response [9]. Interference arises from the sample matrix that inherently contains a mixture of electrolytes, and from exogenous compounds. In the latter case, accurate ion sensing becomes even more challenging since the target electrolyte is extremely diluted in

the biological fluid. Therefore, interference constrains potentiometric sensors to be highly selective towards their target ion. Major advancements are made in ion sensing technology to increase sensor selectivity, but the sensors proposed in literature cannot actually cope with intrinsic electrolyte cross-selectivity bounds. An alternative is to increase the prediction accuracy of the concentration of target electrolytes downstream, with efficient data processing and learning algorithms [10]. Multi-ion sensing requires a multivariate calibration model to bind sensor array responses to target ions concentrations [11]. Chemometric methods include linear inverse least-squares models, but the strong non-linearity observed in presence of interferent ions suggest the use of non-linear regression models such as *Artificial Neural Networks* (ANNs) [12] [13]. However, these models necessitate large training dataset in the calibration and validation phase in order to get good prediction accuracy. A batch of sensor calibration, with different ion mixture combinations is typically needed. Unfortunately, acquiring this large amount of data is time and resource consuming in practice.

Thus, in the present work, a calibration-curve generator is proposed to emulate multi-ion sensing in presence of interferent ions. First, the tool is used for investigation, allowing us to understand the impact of sample composition and membrane selectivity in the sensor response. Moreover, the emulator is implemented to generate mixed-ion synthetic dataset to be fed to ANN models in a multivariate calibration framework. The analytical description and assumptions of the ion sensing models used are detailed in Section II. Then, the parameters of the calibration-curve emulator are described in Section III, highlighting the versatility of the tool. Next, a methodology for generating synthetic ion sensing dataset is presented in Section IV. The conclusions are reported in Section V.

## II. ION SENSING MODELING

In potentiometric ion sensing, all-solid-state *ion-selective electrodes* (ISEs), coated with an ion-selective membrane, transduce the thermodynamic activity of the target ion into an electrical potential. Namely, the *open circuit potential* (OCP) between the ISE and an inert reference electrode, that has a stable potential, is measured under quasi-zero current conditions [14]. Sensor calibration is performed to link OCP sensor response and the target ion activity. The latter describes the ability of the analyte to react with other ions, and it

is related to the effective ion concentration by the activity coefficient. In the following, ion activity is referring to the chemical property tracked in electrolyte sensing.

Nicolsky-Eisenmann model is commonly used to describe the response of ion sensors. Nevertheless, large deviations from acquired sensor data are observed with sensor arrays put in presence of ion mixtures [15]. In this work, the phase-boundary potential model is used to derive the Nernstian response of a polymeric membrane ISE in mixed-ion solutions. A general description of the model could be found in [16]. The hereunder analytical derivation is carried out to get a compact modeling of ISE response, with the most relevant sensor properties chosen as design parameters. The phase-boundary potential model is based on ion-exchange equilibrium considerations at the sample/membrane interface. An electrical potential difference is built up at the interface to counter-balance the ion fluxes from the sample phase to the membrane phase, where the target ion is entrapped. Nernst equation links the phase-boundary potential  $E_{PB}$  to the activity of the target ion in the sample,

$$E_{PB} = \epsilon_j^0 + \frac{1}{z_j} \cdot s \cdot \log \left( \frac{a_j(m)}{a_j(aq)} \right) \quad (1)$$

where  $\epsilon_j^0$  is the standard potential of ion  $j$  of valence  $z_j$ ,  $s$  is the Nernst slope, and  $a_j(m)$ ,  $a_j(aq)$  are the activities of ion  $j$ , in the membrane, and the sample, respectively. Then, considering the ion-selective membrane (consisting of ionophore and ion-exchanger), it is assumed that the changes in the activities of uncomplexed ionophore and extracted ions during ion exchange are negligible. The electroneutrality of the membrane, for multiple ions in the membrane and the sample phases, yields

$$10^{-z_j \cdot E_{PB}/s} \sum_j a_j(aq) \cdot 10^{z_j \cdot E_j^0/s} = 1 \quad (2)$$

where  $E_j^0$  is introduced as the apparent standard potential of ion  $j$ . It includes  $\epsilon_j^0$  and the parameters of the ionophore and ion-exchanger. Then, the selectivity coefficient is defined as  $\log K_{I,J}^{pot} = \frac{z_I}{s} \cdot (E_j^0 - E_I^0)$ . It quantifies how much a membrane is selective towards the target ion  $I$  than an interferent ion  $J$ . As a result, the following compact equation is obtained, considering only monovalent and divalent ions in the sample matrix.

$$\begin{aligned} & 10^{z_I(E_I^0 - E_{PB})/s} \cdot a_I(aq) \\ & + 10^{(E_I^0 - E_{PB})/s} \sum_{j \text{ s.t. } z_j=1} (K_{I,j}^{pot})^{\frac{1}{z_I}} \cdot a_j(aq) \\ & + 10^{2(E_I^0 - E_{PB})/s} \sum_{j \text{ s.t. } z_j=2} (K_{I,j}^{pot})^{\frac{2}{z_I}} \cdot a_j(aq) = 1 \end{aligned} \quad (3)$$

The first contribution is given by the target ion  $I$ , while the two sums account for monovalent and divalent interferent ions, respectively. Selectivity coefficients could be seen as

weighting factors of the activity of interferent electrolytes. Next, Equation 3 is solved for  $E_{PB}$ , and yields

$$E_{PB} = E_I^0 + s \cdot \log \left( f(a_I, \{(a_{J_1}, K_{I,J_1}^{pot}), \dots (a_{J_l}, K_{I,J_l}^{pot})\}_{z_{J_i}=1}, \{(a_{J_1}, K_{I,J_1}^{pot}), \dots (a_{J_m}, K_{I,J_m}^{pot})\}_{z_{J_i}=2}) \right) \quad (4)$$

where  $f$  is a highly non-linear function of the activity and selectivity coefficients of the constituents. An ideal Nernstian response is retrieved if  $f = a_I$ . Eventually, the measured OCP at ion  $I$ -ISE is  $E_I = K_{cell} + E_{PB}$ , where  $K_{cell}$  is a constant accounting for the other potentials in the galvanic cell.

### III. CALIBRATION-CURVE EMULATOR

The ion sensing model previously described is used to emulate ISE responses in different sample compositions. A calibration-curve emulator is designed for this purpose, enabling the quantification of the impact of sample composition, interferent ions and membrane selectivity, in different ion mixture solutions. The *graphical user interface* (GUI) displayed in Fig. 1 is built in PyQt5 to automate simulations.

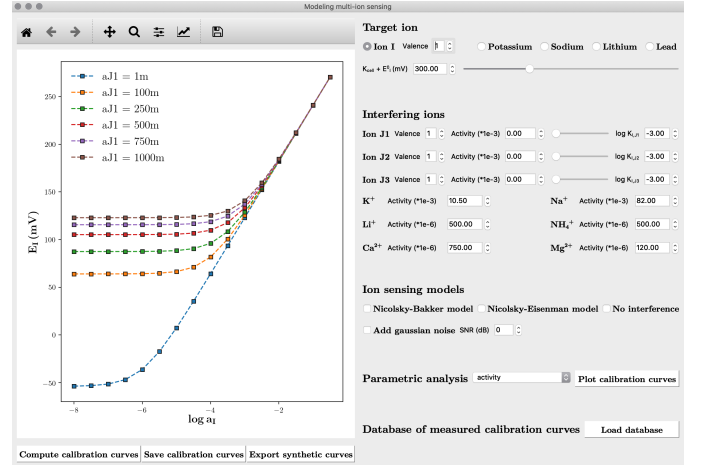


Fig. 1: GUI developed to generate synthetic calibration curves in different mixed-ion solutions, to perform parametric simulations, and to compare synthetic curves with database of in-vitro calibration curves.

The main parameters of the GUI are detailed in the following.

- **Target ion  $I$ :**  $I \in \{\text{potassium, sodium, lithium, lead}\}$  is selected. Monovalent/divalent ion  $I$  could be used for standard simulation.
- **Offset:**  $K_{cell} + E_I^0$  is modeled as an offset potential. It depends on the primary ion, takes into account membrane composition and sample-independent potentials such as reference electrode potential, potential drops at the electrodes.
- **Interfering ions  $J_k$ :** multi-ion sensing in sweat involve  $J_k \in \{\text{potassium, sodium, lithium, ammonium,}$

calcium, magnesium}. The physiological activity of these ions in sweat are used by default. Cross-selectivity coefficients are taken from literature, and are reported in Table 1. For standard simulation with target ion I, ions  $J_1, J_2, J_3$ , with selectable valence, activity, and selectivity coefficient are the interferent electrolytes.

TABLE 1: Cross-selectivity coefficients of the constituents considered in sweat sample. Values are extracted from literature (fixed interference method, [17] [18]).

		$\log K_{I,J}^{\text{pot}}$						
I \ J		$K^+$	$Na^+$	$Li^+$	$Pb^{2+}$	$NH_4^+$	$Mg^{2+}$	$Ca^{2+}$
$K^+$		1	-1.7	-2.3	-	-0.5	-3.2	-
$Na^+$		-1.8	1	-2.5	-	-2.8	-4.2	-3.7
$Li^+$		-2.65	-2.26	1	-	-3.18	-4.52	-3.91
$Pb^{2+}$		-5.6	-5.8	-5.6	1	-2.12	-6.2	-6.2

- **Ion sensing models:** phase-boundary potential model (Nicolosky-Bakker) and Nicolosky-Eisenmann model are used to simulate the ISE response with the ion mixture scenario set. Theoretical full-Nernstian response is plotted to assess the amount of potential distortion due to interference. Gaussian noise could be added to the synthetic curve, tuned as equivalent sensor signal-to-noise ratio.
- **Parametric analysis:** parametric sweep of the activity and selectivity coefficient of the interferent ion could be done. Typical calibration curves are displayed in Fig. 2. It quantitatively explains the impact of interference in the ISE response. For poorly selective sensors and ISEs in presence of concentrated interferent ions, the background potential (potential at  $\log a_I \rightarrow -\infty$ ) rises, and the elbow of the calibration curve shifts towards higher activities. The lower *limit of detection* (LOD) of the sensor is extrapolated as the primary ion activity at the intersection of the linear Nernstian sensor response and the flat background potential. Therefore, the lower LOD increases in presence of concentrated interfering ions. This could be critical if the lower LOD reaches the physiological range of concentration of the primary ion in sweat.
- **Load database of calibration curves:** calibration curves obtained from in-vitro measurements could be loaded to compare synthetic and measured calibration curves, as illustrated in Fig. 3. The database is obtained with commercial platinum screen-printed electrodes (Sigma Aldrich, Switzerland) nanostructured according to [19], and coated with ionophores following recommended cocktail composition by Sigma Aldrich. The OCPs of the prepared ISEs are measured with an Autolab potentiostat (Metrohm, Switzerland) against a double-junction Ag/AgCl reference electrode (Metrohm). By tuning the model parameters, it is possible to fit synthetic calibration curves to acquired sensor data. This procedure enables the extraction of sensor parameters as well, that are used to produce more realistic synthetic dataset in the following.

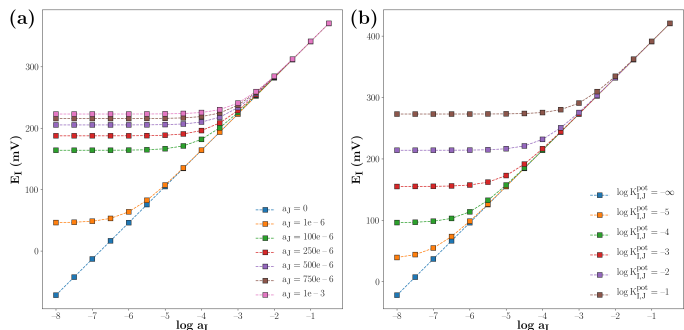


Fig. 2: Parametric analysis of multi-ion sensing: (a)  $a_j$  swept from 0 to  $1e-3$ , with  $z_I = 1$ , offset = 400 mV,  $z_J = 1$ , and  $\log K_{I,J}^{\text{pot}} = -3$ ; (b)  $\log K_{I,J}^{\text{pot}}$  swept from  $-\infty$  to  $-1$ , with  $z_I = 1$ , offset = 450 mV,  $z_J = 1$ , and  $a_j = 10e-6$ .

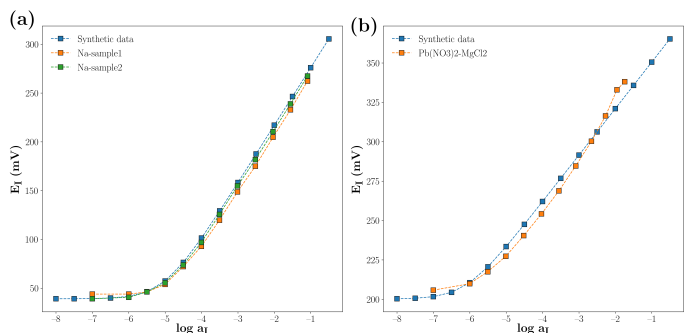


Fig. 3: Fitting synthetic and measured calibration curves: (a) sodium sensor calibration, (b) lead sensor calibration with magnesium as interferent ion.

- **Export calibration curves:** synthetic calibration curves are exported as text files and png images.

#### IV. DESIGN OF SYNTHETIC DATASET

The ion sensing models described are used to generate synthetic OCP responses in different mixed-ion solutions. 7 constituents are considered in the sample matrix: potassium, sodium, lithium, lead, ammonium, magnesium, and calcium ions. A 4-channel ISE array sensing the first 4 ions is emulated with different sample compositions. The determination of different ion mixtures combinations is a multifactor design of experiments. Taguchi method is implemented to generate a representative subset of all constituents combinations with orthogonal arrays [20]. The range of activities of the 7 factors are quantized in 6 levels summarized in Table 2. They are set according to their physiological range in sweat. A  $L_{18}(6^1 \times 3^6)$  orthogonal array is implemented in which the 6-level factor is cyclically permuted over the 4 primary constituents, given that column permutation preserves orthogonality. A default nominal sample composition is also added in the dataset. Thus, 145 non-redundant synthetic mixtures are obtained. It is large enough for training and validation of chemometric models. For comparison, 31 and 52 real ion mixtures are prepared in the

multivariate calibration frameworks using ANNs, in [12] and [13], respectively.

TABLE 2: Discrete activity levels of the constituents. The target ions are in *italic*.

Level	Activity of each factor ( $\times 1e - 3$ )						
	<i>K<sup>+</sup></i>	<i>Na<sup>+</sup></i>	<i>Li<sup>+</sup></i>	<i>Pb<sup>2+</sup></i>	<i>NH<sub>4</sub><sup>+</sup></i>	<i>Mg<sup>2+</sup></i>	<i>Ca<sup>2+</sup></i>
L1	0.1	0.1	0.05	0.001	0.01	0.01	0.01
L2	0.5	1	0.1	0.01	0.05	0.05	0.05
L3	1	5	0.25	0.05	0.1	0.1	0.1
L4	5	50	0.5	0.1	0.25	0.25	0.25
L5	10	100	1	0.25	0.5	0.5	0.5
L6	20	150	2.5	0.5	1	1	1

Next, the simulated responses of the 4 ISEs with the 145 samples are computed. This is automated by a tool that takes any orthogonal table of 7 factors as input, and outputs the corresponding 4-dimensional OCP responses. The parameters of the emulator are the quantized activity of Table 2, the offset potential of each sensor, and the cross-selectivity coefficients between constituents of Table 1. The synthetic OCP responses are displayed in Fig. 4. It is observed that lead and sodium detection is weakly affected by interferent ions. Indeed, lead membrane are particularly selective. Conversely, there is a large OCP dispersion for lithium detection, and for potassium detection, in diluted analyte. Sensor calibration in these two cases necessitates non-linear chemometric methods.

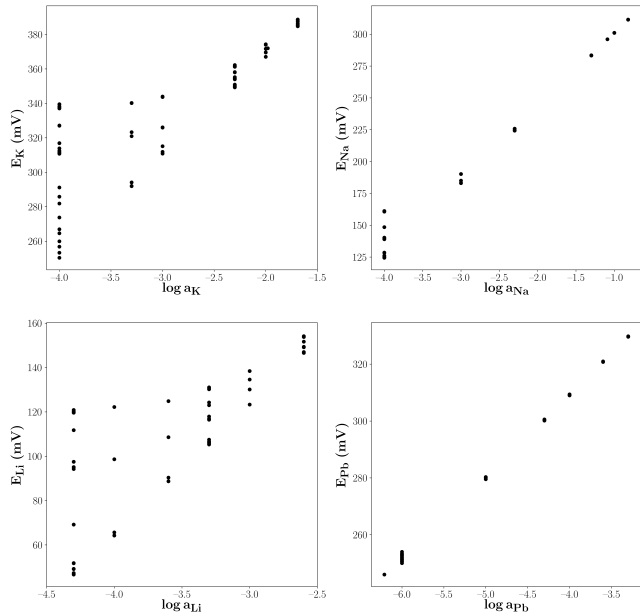


Fig. 4: Visualization of synthetic OCP/activity dataset, obtained through orthogonal design of experiments emulating a 4-channel ISEs monitoring.

## V. CONCLUSION

In this work, a compact model of the phase-boundary potential at the sample/membrane interface is derived to be the basis of a mixed-ion sensing emulator. The impact of

interference and sensor selectivity on sensor lower LOD is quantified by the distortion of the calibration curves from an ideal Nernstian behaviour. Next, 4-channel ions monitoring is emulated using an orthogonal design of the sample composition. This allows us to simulate sensor array response with different ion mixtures that are representative of electrolytic composition of sweat during physical exercise or ion intake. A tool is developed to automate the generation of the synthetic dataset. Ongoing work is focusing on chemometric models to implement multivariate calibration on the multi-dimensional OCP/activity dataset. These methods include inverse least-squares and ANN models.

## ACKNOWLEDGEMENT

This research is supported by H2020 ERC 2014 ADG 669354 CyberCare. The authors would like to thank Francesca Criscuolo for providing database of calibration curves with the ion sensors she is developing.

## REFERENCES

- [1] M. Parrilla, M. Cuartero, and G. A. Crespo, "Wearable potentiometric ion sensors," *TrAC - Trends in Analytical Chemistry*, vol. 110, pp. 303–320, 2019.
- [2] M. Bariya, H. Y. Y. Nyein, and A. Javey, "Wearable sweat sensors," *Nature Electronics*, vol. 1, no. 3, pp. 160–171, 2018.
- [3] S. J. Montain, S. N. Cheuvront, and H. C. Lukaski, "Sweat mineral-element responses during 7 h of exercise-heat stress," *International Journal of Sport Nutrition and Exercise Metabolism*, vol. 17, no. 6, pp. 574–582, 2007.
- [4] D. B. Speedy, T. D. Noakes, and C. Schneider, "Exercise-associated hyponatremia: A review," *Emergency Medicine*, vol. 13, no. 1, pp. 17–27, 2001.
- [5] R. Klesges, K. Ward, M. Shelton, and et al., "Changes in bone mineral content in male athletes: Mechanisms of action and intervention effects," *JAMA*, vol. 276, no. 3, pp. 226–230, 1996.
- [6] J. Cohn and E. Emmett, "The excretion of trace metals in human sweat," *Annals of Clinical and Laboratory Science*, vol. 8, no. 4, 1978.
- [7] A. Muneer, "Staging Models in Bipolar Disorder: A Systematic Review of the Literature." *Clinical psychopharmacology and neuroscience : the official scientific journal of the Korean College of Neuropsychopharmacology*, vol. 14, no. 2, pp. 117–30, 2016.
- [8] M. I. Ny Hanitra, F. Criscuolo, S. Carrara, and G. De Micheli, "Multi-target electrolyte sensing front-end for wearable physical monitoring," in *2019 15th Conference on Ph.D Research in Microelectronics and Electronics (PRIME)*, 2019, pp. 249–252.
- [9] G. Dimeski, T. Badrick, and A. S. John, "Ion Selective Electrodes (ISEs) and interferences-A review," *Clinica Chimica Acta*, vol. 411, no. 5-6, pp. 309–317, 2010.
- [10] R. B. D. Cruz, G. A. Alonso, R. Muñoz, and J.-L. Marty, *Biosensors: Recent advances and mathematical challenges*. OmniaScience, March 2014, ch. Continuous monitoring based on biosensors coupled with artificial intelligence, pp. 143–161.
- [11] A. C. Olivieri, *Introduction to Multivariate Calibration*. Springer, 2018.
- [12] L. Wang, Y. Cheng, D. Lamb, Z. Chen, P. J. Lesniewski, M. Megharaj, and R. Naidu, "Simultaneously determining multi-metal ions using an ion selective electrode array system," *Environmental Technology and Innovation*, vol. 6, pp. 165–176, 2016.
- [13] L. Nuñez, X. Cetó, M. I. Pividori, M. V. Zononi, and M. del Valle, "Development and application of an electronic tongue for detection and monitoring of nitrate, nitrite and ammonium levels in waters," *Microchemical Journal*, vol. 110, pp. 273–279, 2013.
- [14] J. Hu, A. Stein, and P. Buhlmann, "Rational design of all-solid-state ion-selective electrodes and reference electrodes," *TrAC - Trends in Analytical Chemistry*, vol. 76, pp. 102–114, 2016.
- [15] M. Nägele, E. Bakker, and Pretsch, "General description of the simultaneous response of potentiometric ionophore-based sensors to ions of different charge," *Analytical Chemistry*, vol. 71, no. 5, pp. 1041–1048, 1999.

- [16] E. Bakker, "Generalized Selectivity Description for Polymeric Ion-Selective Electrodes Based on the Phase Boundary Potential Model," *Journal of electroanalytical chemistry (Lausanne, Switzerland)*, pp. 1–20, 2011.
- [17] K. Suzuki, "Design and synthesis of sodium ion-selective ionophores based on 16-crown-5 derivatives for an ion-selective electrode," *Analytical Chemistry*, vol. 68, no. 1, pp. 208–215, 1996.
- [18] Wardak, C. and Lenik, J., "New lead-sensitive ion selective electrode with low detection limit," *E3S Web of Conferences*, vol. 1, p. 05010, 2013.
- [19] F. Criscuolo, I. Taurino, F. Stradolini, S. Carrara, and G. D. Micheli, "Highly-stable li+ ion-selective electrodes based on noble metal nanostructured layers as solid-contacts," *Analytica Chimica Acta*, vol. 1027, pp. 22 – 32, 2018.
- [20] R. Kacker, E. Lagergren, and J. Filliben, "Taguchi's orthogonal arrays are classical designs of experiments," *Journal of Research of the National Institute of Standards and Technology*, vol. 96, no. 5, p. 577, 1991.